IEEE Access
Multidisciplinary ⋮ Rapid Review ⋮ Open Access Journal

Received 13 September 2023, accepted 23 October 2023, date of publication 25 October 2023, date of current version 1 November 2023.

Digital Object Identifier 10.1109/ACCESS.2023.3327526

RESEARCH ARTICLE

A Low-Profile, Electrically Small Ferrite Core-Loaded Grounded Split Ring Resonator Antenna for Military VHF/UHF Communication

MEE-SU LEE[1], (Student Member, IEEE), WONKYO KIM[1], (Graduate Student Member, IEEE), GEONYEONG SHIN[2], HYUN KIM[2], CHANG-HYUN LEE[2], AND ICK-JAE YOON[1], (Senior Member, IEEE)

[1]Department of Electrical Engineering, Chungnam National University, Daejeon 34134, Republic of Korea
[2]LIG Nex1 Company Ltd., Yongin 16911, Republic of Korea

Corresponding author: Ick-Jae Yoon (ijyoon@cnu.ac.kr)

This work was supported by the Challenging Future Defense Technology Research and Development Program of Agency for Defense Development, in 2019, under Grant 9127786.

ABSTRACT This study proposes a low-profile, electrically small military VHF/UHF communication ferrite-loaded antenna for an integrated mast (IM). We realized a relatively lighter weight antenna that is advantageous for IM mounting by utilizing a minimum number of ferrite cores. The proposed antenna is in the form of a ferrite-loaded split ring resonator-shaped grounded loop structure that exhibits exceptional radiation performance at an electrically small size. The size of the proposed antenna with the assembled housing for IM mounting is $970 \times 429 \times 47.5$ [mm^3], representing a very small electrical size *ka* of 0.34 with respect to the lowest operating frequency of 30.4 MHz, with a criterion VSWR of less than 3. The entire profile is extremely thin as 0.005λ. The minimum measured realized gain is -14.5 dBi, indicating an upward trend along the matched frequency of up to 500 MHz.

INDEX TERMS Ferrite core, low-profile, electrically small antenna, split ring resonator, integrated mast.

I. INTRODUCTION

The evolution of naval warfare into electronic warfare (EW), which synthesizes the surveillance and reconnaissance of information to conduct engagements and joint operations is underway. Therefore, multiple antennas that communicate, collect tactical information, and perform missions are mounted on battleship masts. Thus far, these types of antennas have been placed high on masts, operating individually, as shown in Fig. 1a, represented by a dashed yellow circle [1]. Although multiple antennas are grouped in a physically narrow space, the entire system remains heavy and requires considerable space. This arrangement results in unwanted electromagnetic interference from scattering, contradicting the recent trend of lightweight and compact antenna designs [2], [3], [4]. Recently, an integrated mast (IM) as a shared aperture antenna, where multiple antennas for radar, EW, and communication are integrated into a single flat platform has been investigated, as shown in Fig. 1b [5], [6]. An IM has a lower radar cross-section (RCS) than a conventional mast. Additionally, military communication antennas generally operate in the VHF/UHF band (30–500 MHz) and have a pole shape of 1–3 m to operate over a wide frequency band with vertical polarization with respect to the sea surface [7], [8], [9]. However, such a pole-type antenna causes low mobility with an increased RCS level. Consequently, conventional pole-type communication antennas are not suitable for IM; however, lightweight, miniaturized, yet low-profile antennas that show vertically polarized radiation over an ultra-widely matched impedance frequency are highly desired.

Thus, we propose a low-profile, relatively lighter weight, ferrite core-loaded, wideband VHF/UHF communication

The associate editor coordinating the review of this manuscript and approving it for publication was Pavlos I. Lazaridis.

(a) (b)

FIGURE 1. Mast of a naval ship. (a) Conventional mast. (b) Integrated mast.

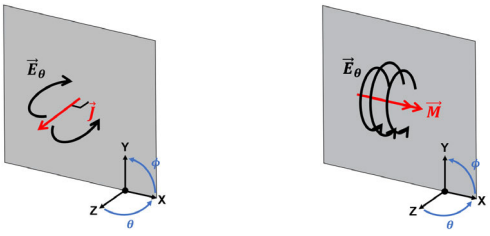

(a) (b)

FIGURE 2. Radiation source on a conducting surface with the associated electric field. (a) Electric current source. (b) Magnetic current source.

antenna design based on a metamaterial-inspired split-ring resonator (SRR) structure for IM. We utilize ferrite tiles at the core of the antenna for a permeable, self-grounded loop design enabling an efficient loop current distribution to achieve wide frequency operation and vertical polarization characteristics in a planar and low-profile form factor. For further miniaturization, we modify the basic design by inserting a grounded conductor structure between the top and bottom of the conductor parts, which give the proposed design the resonant property of an SRR. This work is further developed from the VHF communication antenna in [10] with the improvement in the overall weight and performance. The proposed design is covered with a polycarbonate (PC) housing for a firm assembly, resulting in overall antenna dimensions of $970 \times 429 \times 47.5$ [mm^3], satisfying the lowest operating frequency of 30.4 MHz with a reference VSWR of less than 3. The electrical size ka and profile are 0.34 and 0.005λ, respectively. The design procedure and working mechanism of the proposed VHF/UHF communication antenna are explained through full-wave electromagnetic simulations utilizing the CST studio suite. We conducted experiments and achieved a realized gain of -14.5 dBi at the lowest matched frequency of 30.4 MHz in the elevation plane while showing a generally upward increasing trend of up to 500 MHz. Vertical polarization characteristics were also observed over the entire frequency band.

II. DESIGN CONSTRAINTS AND STRATEGY

A. Q-FACTOR ANALYSIS ACCORDING TO THE FORM FACTOR OF A RADIATING SOURCE

In [11], the radiating quality factor (Q) was calculated based on the source type and structure to examine the Q bounds for arbitrarily shaped radiators. They defined the aspect ratio (AR) of an electrically small perfect electric conductor (PEC) structure as the height-to-width ratio. An AR less than one indicates a low-profile case or a bar-shaped dipole, whereas an AR above one implies a pole-type dipole. A comparison of the Q values according to the AR of the radiator (Figs. 9 and 10 in [11]), it is found that the magnetic dipole shows a relatively lower Q than the electric dipole in the low-profile region. However, in regions with AR greater than 1, Q is inverted, indicating that a magnetic dipole is more appropriate for a lower-Q planar design.

Furthermore, the current source can effectively radiate when an electric and a magnetic source are located above the PEC ground like in Figs. 2a and 2b, respectively. The magnetic source in Fig. 2b shows the longitudinal electric field distribution, enabling a vertical polarization operation.

B. CHARACTERISTIC MODE ANALYSIS

Characteristic mode analysis (CMA) is the numerical expansion of currents and electric fields scattered or radiated by an arbitrary object, providing physical insight into the source-free structure of radiation. It has been widely used in designing antennas considering installation platforms [12], [13], [14], [15], [16] because it can be used to determine the efficient excitation source type and radiation mode of the antenna.

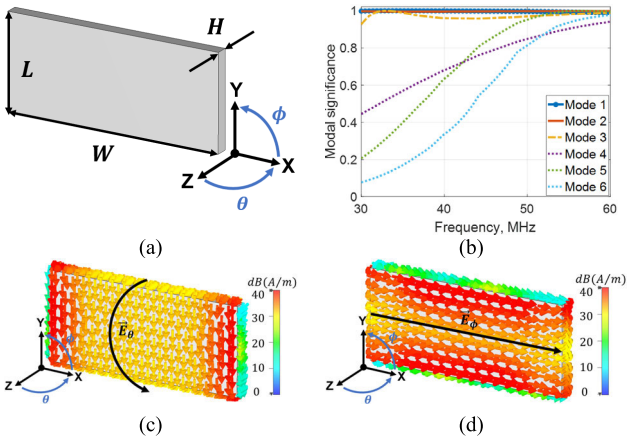

(a) (b) (c) (d)

FIGURE 3. Modal significance of the bar-shape conductor structure. (a) Geometry of the conductor structure ($W = 900$, $L = 370$, and $H = 50$ [mm]). The ground plane is not shown. (b) Modal significance. (c) Surface current distribution of Mode 1. (d) Surface current distribution of Mode 2.

The CMA was performed as shown in Fig. 3. A low-profile bar-shaped PEC structure with an AR (H/W) below 0.2 was located above a sufficiently large PEC ground as shown in Fig. 3a because the communication antenna will be placed as a part of the IM. The CMA simulations were performed without additional excitation. The modal significance (MS)—a parameter that indicates the modes that can most efficiently resonate for a given structure—ranging from 0 to 1 can be obtained from this analysis. The mode

resonates and radiates most effectively when MS equals 1. As shown in Fig. 3b, where the MSs of the conductor in Fig. 3a are plotted, modes 1 and 2 show values close to 1 starting from 30 MHz. The corresponding modal current distributions of each mode are presented in Figs. 3c and 3d, respectively, where the black arrows indicate the direction of the electric field. Mode 1 in Fig. 3c indicates the desired current distribution and electric field in the θ direction, whereas Mode 2 in Fig. 3d indicates a dominant current flow in the φ direction. Therefore, this shape of the conductor bar could be promising for a low-profile antenna design with vertical polarization for IM as long as it is properly fed for exciting Mode 1.

However, the magnetic dipole experiences twice higher radiating Q than an electric dipole of the same electrical size [17], [18]. To resolve this problem, ferrite has been utilized as a resonant core to design efficient wideband loop antennas [19], [20]. Conventional studies on these ferrite applications primarily utilized low-loss ferrite to improve the radiation efficiency of a loop antenna [21], [22]. However, the magnetic loss must not be a relevant constraint in designing an efficient loop from the calculation of the radiation efficiency of an antenna by considering the complex permeability of ferrite with no approximation [23]. Thus, in contrast to the conventional concepts, a highly efficient loop antenna can be designed using a high-loss ferrite core.

For the proposed design, we chose the self-grounded loop in Fig. 4 as a starting point to encounter the findings from the Q-factor and CMA analyses, which should provide a loop current distribution similar to a magnetic dipole source on the ground plane. Additionally, a ferrite core was filled inside the loop for miniaturization and wideband operation of the antenna. In practice, the antenna can be fed using a coaxial cable from the bottom of the ground ($z < 0$) without requiring a balun.

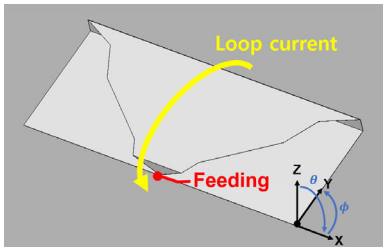

FIGURE 4. Self-grounded loop antenna.

III. ANTENNA DESIGN

A. WIDEBAND, ELECTRICALLY SMALL ANTENNA DESIGN USING A FERRITE CORE

For the ferrite tiles, we chose the M28 series tile from Laird as the antenna core, as it can provide high permeability in the frequency range of 30–600 MHz [24]. The dimension of a single tile is 53 × 53 × 2.5 [mm^3] and is placed in a space of 901 × 318 [mm^2] under the upper conductor, creating a self-grounded loop antenna, as shown in Figs. 5a and 5b, in which the top and side views of the antenna are shown, with the conductor and ferrite represented by white and grey colors, respectively. Next, we varied the height of the tile layer by 50, 30, and 10 mm, as shown in Fig. 5b, and the VSWR according to the height of the tile is shown in Fig. 5c. The lowest operating frequency shifted upward with a thinner ferrite core profile. The number of ferrite tiles utilized and electrical size of the antenna are inversely proportional; thus, a smaller design could be obtained with a larger number of ferrites. However, because we intended to utilize considerably few ferrite tiles for lighter IM designs, further study of the conductor part of the antenna is required to reduce the lowest operating frequency. Note that, the number of tiles and their weight are 408 pieces and 14.3 kg, respectively, with a ferrite core height of 10 mm. Aluminum was utilized as the conductor.

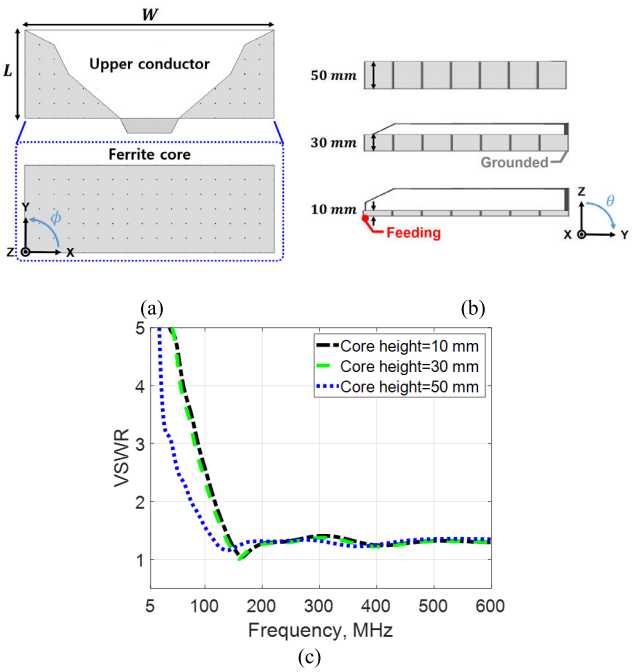

FIGURE 5. VSWR simulation results according to the ferrite core height. (a) Basic model of the proposed antenna (W = 901, L =318 [mm]). (b) Side view of the antenna with respect to the ferrite core height. (c) VSWR simulation results.

B. IMPEDANCE MATCHING STRUCTURE: SPLIT-RING RESONATOR

The operating frequency can be lowered by adding capacitance to the antenna structure. Consequently, we inserted a grounded conductor (marked by a dashed box in Fig. 6a) between the upper conductor and ground, as shown in Fig. 6a. From the side view of the antenna, the entire structure with the added conductor resembles a half-cut of the well-known SRR. Using a method of image, a schematic of the current distribution owing to the inserted conductor could be added, as shown in Fig. 6b.

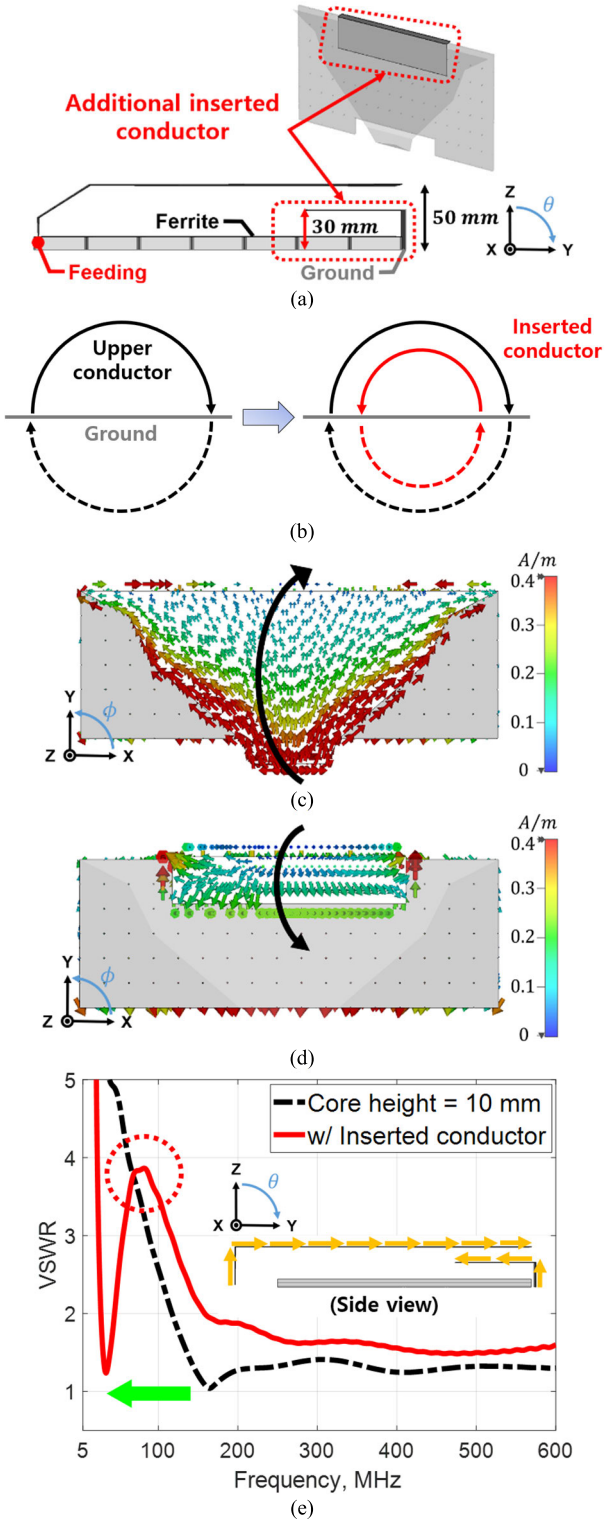

FIGURE 6. Impedance matching enhancement. (a) Antenna with an additional inserted conductor. (b) Conceptual image of the current distribution owing to the additional inserted conductor. (c) Surface current distribution of upper conductor at 60MHz. (d) Surface current distribution of inserted conductor at 60MHz. (e) VSWR of the antenna.

The surface current distributions of each upper and inserted conductor at 60 MHz are shown in Figs. 6c and 6d, where the opposite current direction in the upper and inserted conductors is clearly observed, like those in the neighbor conductors of an SRR that are flipped with respect to each other. The current distribution from the side view of the antenna is visualized inset to Fig. 6e for the clarity of understanding. In Fig. 6e, the VSWRs of the modified design with the inserted conductor, that is, the SRR-shaped antenna, are indicated by a red solid line. The lowest operating frequency shifted downward (represented by a green arrow) owing to the improved loop current distribution from the metamaterial inspired SRR unit cell configuration [25, see Fig. 8]. Some outstanding problems, such as the unmatched region (marked by a red dashed circle) and practical fabrication are discussed in the next section.

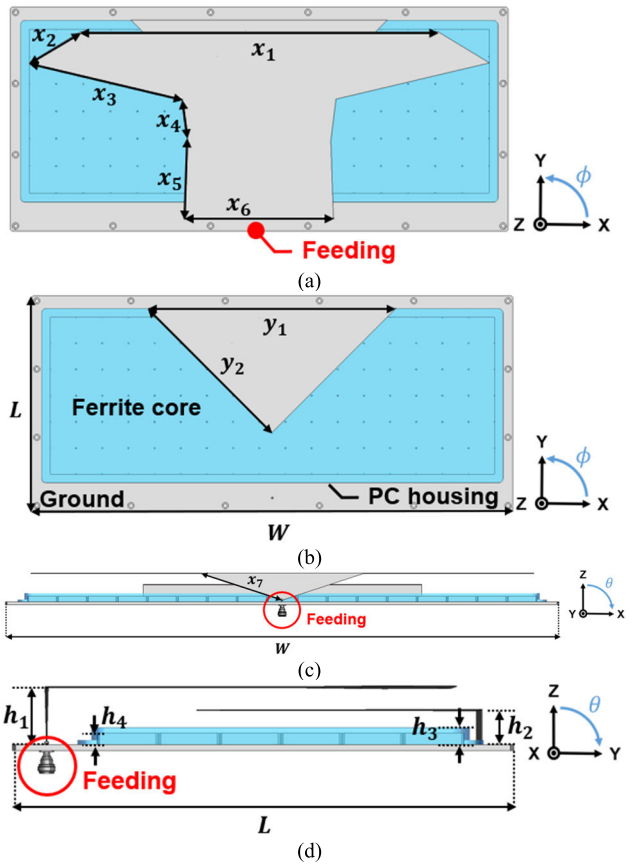

FIGURE 7. Final design of the proposed antenna. (a) Top view of the upper conductor. (b) Top view of the inserted conductor. (c) Front view. (d) Side view.

C. FINAL DESIGN OF THE PROPOSED ANTENNA

The final optimized design of the proposed ferrite-cored SRR -shaped antenna is shown in Fig. 7. The proposed antenna is composed of the upper and inserted conductors as well as the ground. They are shown in the light-grey color. Underneath these conductors is a ferrite core, which is held in place by a PC-based dielectric housing ($\varepsilon_r = 3.4$), shown in light blue. The PC housing was designed to rigorously support the ferrite cores such that the prototype is stable during

TABLE 1. Design parameters and values of the proposed antenna.

Parameter	Value	Parameter	Value
W	970	$x7$	153
L	429	$y1$	500
$x1$	700	$y2$	354
$x2$	117	$h1$	47.5
$x3$	308	$h2$	30.5
$x4$	106	$h3$	16
$x5$	159	$h4$	10
$x6$	263		

Note: All units are in millimeters.

outdoor measurements. The shape of the upper conductor in Fig. 7a was optimized to improve the impedance-matching characteristic across the entire operating frequency band and was fed by a coaxial cable from beneath the ground, as shown in Figs. 7c and 7d. The inserted conductor was triangularly shaped and was grounded on the opposite side of the feed, as shown in Fig. 7b and 7d. As shown in Fig. 7d, the inserted conductor should create a loop current with the ground in a direction opposite to the current flow over the upper conductor and ground plane. The overall structure resembles a grounded SRR, which allowed more capacitance and denser current distribution to the antenna. The ferrite cores and M28 series tiles from Laird used in the simulation were stacked at a height of 10 mm on the ground plane. A total of 408 ferrite tiles were placed in a rectangular dimension of a 901 $\times$ 318 [mm^2] space with a total weight of 14.3 kg. The dimensions of the antennas are listed in Table 1. The overall height of the antenna (h_1) is 47.5 mm, denoting 0.005λ at the lowest operating frequency with an electrical size ka of 0.34.

The computed boresight realized gain and VSWR of the final design, considering the assembly parts like in Fig. 9, are plotted in Fig. 8a, when it is placed on a center of a 3 m $\times$ 3 m ground plane. The lowest operating frequency was 30.8 MHz with a criterion of VSWR less than 3, and the lowest gain was -10 dBi at that frequency while exhibiting an upward-increasing trend. In Figs. 8b–8g, $|E_\theta|$ over $|E_\phi|$ is plotted from 30 to 500 MHz, validating the vertical polarization radiation characteristic when the antenna is placed on the ground plane.

IV. EXPERIMENTAL VALIDATION

The optimized proposed VHF/UHF communication antenna model and its prototype configuration, including the bolts and PC housing, are shown in Fig. 9. The conductor parts, including the upper, inserted conductors, and the ground are made of aluminum; the ferrite core above the ground was connected to a PC housing using conductor bolts. The N-type feeder was fixed using a dielectric bracket made of the same PC substrate as the ferrite housing. Because each end of the upper and inserted conductors placed above the ferrite core was in the air, they were supported by Rohacell 71HF

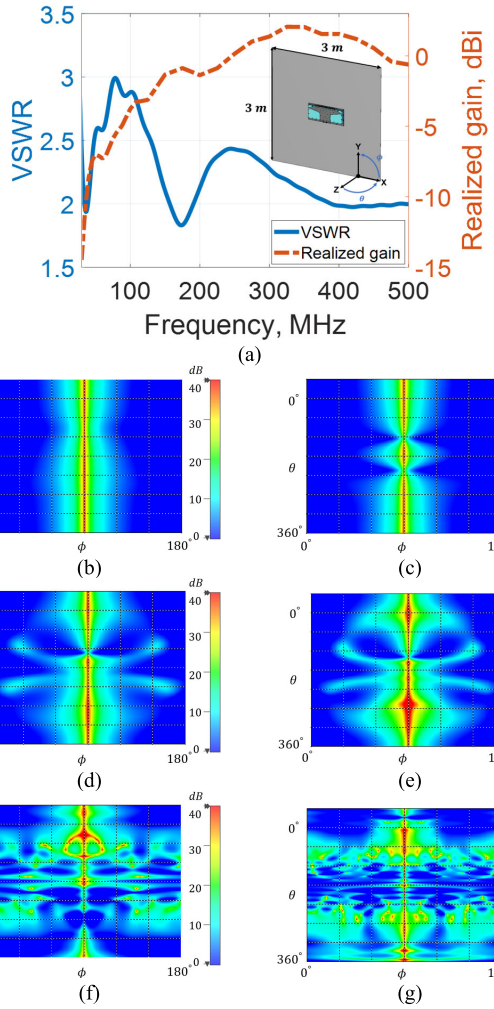

FIGURE 8. Simulation results of the proposed antenna. (a) VSWR and the realized gain. (b) Polarization characteristic ($|E_\theta|$ / $|E_\phi|$) at 30 MHz. (c) Polarization characteristic ($|E_\theta|$ / $|E_\phi|$) at 60 MHz. (d) Polarization characteristic ($|E_\theta|$ / $|E_\phi|$) at 90 MHz. (e) Polarization characteristic ($|E_\theta|$ / $|E_\phi|$) at 100 MHz. (f) Polarization characteristic ($|E_\theta|$ / $|E_\phi|$) at 300 MHz. (g) Polarization characteristic ($|E_\theta|$ / $|E_\phi|$) at 500 MHz.

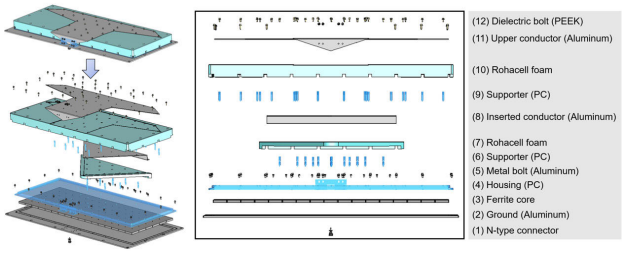

FIGURE 9. Configuration and properties of the built antenna prototype.

(ε_r = 1.075) at positions (7) and (10) as well as the PC supporter in (6) and (9). Dielectric bolts were used in the assembly to minimize their effects on the radiation properties of the antenna. Finally, the conductor and foam were assembled orderly.

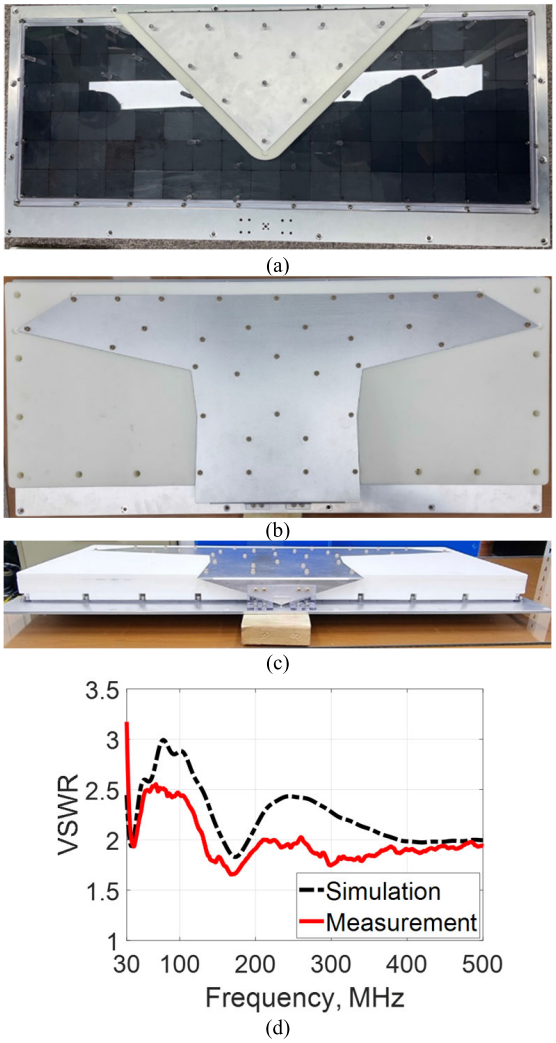

FIGURE 10. Built prototype and VSWR measurement results. (a) Top view of the inserted conductor part and ferrite core with PC housing. (b) Top view of the prototype. (c) Front view of the prototype. (d) Measured results of VSWR.

The photographs of the built prototype and VSWR measurement results are shown in Fig. 10. As shown in Fig. 10a, the triangular inserted conductor was on top of the ferrite core bonded to the transparent PC housing and was supported by the Rohacell foam supporter. Subsequently, the upper conductor and its support structure were sequentially combined and assembled using dielectric bolts. The completed prototype is shown in Figs. 10b and 10c. The measured VSWR results for the prototype are shown in Fig. 10d. The simulated result from Fig. 8a is replotted with a black dashed line as a reference. As shown in this graph, the measured VSWR results of the prototype, represented by the red solid line, generally agree with the simulation results, satisfying the lowest matched frequency of 30.4 MHz with a VSWR criterion of less than 3.

We performed outdoor measurements on the realized gain, radiation pattern and axial ratio as shown in Figs. 11a and 11b because the working frequency of the antenna is as low as 30 MHz. The measurement setup is the same as those used in [10]. The built prototype was located at the center of a perforated 3 m × 3 m steel plate under the same conditions as the simulation environment. It was then lifted to a 17 m-high tower, high enough to minimize the effect of reflections from the earth ground surface. The proposed antenna was utilized as the receiving (Rx) antenna during the measurements. A horizontally polarized log-periodic dipole array antenna was utilized as the transmitting (Tx) antenna. The distance between the Tx and Rx antennas was 250 m. The proposed antenna was rotated by 90° from Fig. 11a for polarization matching with the Tx antenna, as shown in Fig. 11b. A horizontal polarization was utilized during the measurements such that potential interference from the vertically stood measurement tower can be prevented.

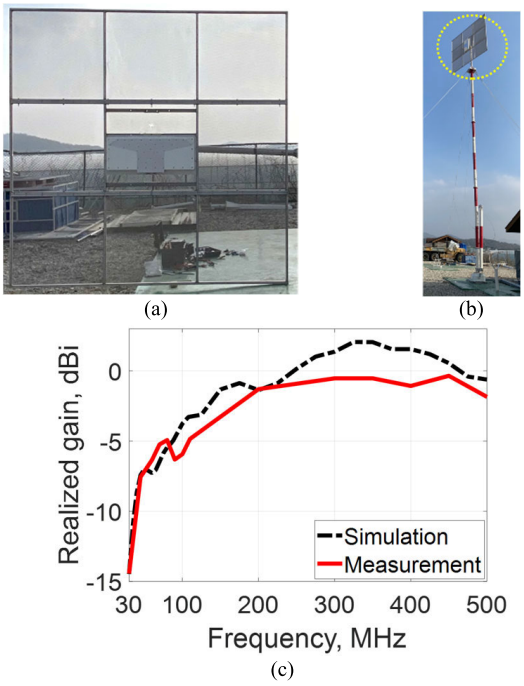

FIGURE 11. Realized gain measurement results. (a) Prototype placed on a 3m×3m ground plane for measurements. (b) Prototype on top of a measurement tower. (c) Simulated and measured results of the realized gain.

The measured realized gain obtained in this manner is shown in Fig. 11c. The measured realized gain satisfied −14.5 dBi at 30.4 MHz, slightly lower than the simulation that is replotted from Fig. 8a for comparison. The deviation might be caused by a slight imperfect polarization match between the Tx and Rx antennas owing to the weight of the prototype and the windy nature of the outdoor measurement. However, the simulated and measured results significantly agree, showing an upward-sloping graph as the frequency increases.

The results of the measured, normalized radiation pattern in an elevation plane according to the frequency, which exhibits characteristics similar to those of the simulations are shown in Figs. 12a–12f. In Fig. 12g, the axial ratio

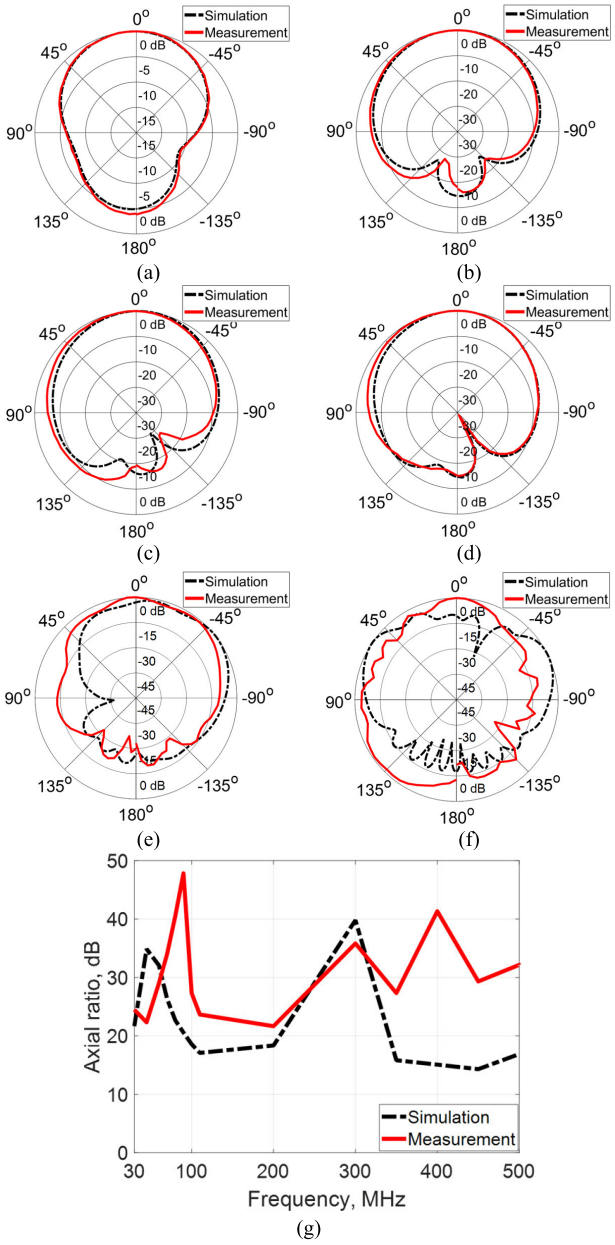

FIGURE 12. Simulated and measured radiation characteristics. (a) Radiation pattern at 30 MHz. (b) Radiation pattern at 60 MHz. (c) Radiation pattern at 90 MHz. (d) Radiation pattern at 100 MHz. (e) Radiation pattern at 300 MHz. (f) Radiation pattern at 500 MHz. (g) Axial ratio ($|E_\theta| / |E_\phi|$). The radiation patterns are normalized.

of $|E_\theta| / |E_\phi|$ in the direction of maximum gain is plotted. Based on the result, $|E_\theta|$ is at least 21 dB higher than $|E_\phi|$ over a wide frequency band, making it suitable for vertical polarization operation.

Lastly, Table 2 compares the operating frequency band, size, weight, and minimum realized gain of the proposed antenna with the ferrite utilized antennas in the literature. Compared to the previous design [10], the proposed antenna is matched from a lower frequency thus having smaller *ka* by about 17% while showing improved radiation performance over wider frequencies including the UHF band. The realized

TABLE 2. Comparison between previously reported ferrite core-loaded antennas and this research.

Ref.	Frequency band [MHz]	Size (W×L×H) [mm^3]/ Weight [kg]	*ka*	Min. realized gain [dBi]
[10]	36.8–300	975×434×62 51.0	0.41	-13
[23]	30–300	1020×100×40 -	0.32	-25
[26]	60–300	430×610×50 9.07	0.47	-15
[27]	90–300	636×112×8.0 1.45	0.61	-15
This work	30.4–500	970×429×47.5 23.0	0.34	-14.5

Note: The values are from the measured results. The electrical size has been calculated with respect to the lowest matched frequency (VSWR<3).

gain of the proposed antenna at 36.8 MHz is -10.8 dBi whereas that of [10] at 30 MHz is -17.0 dBi, from the measurement. In addition, the weight of the utilized ferrite is reduced from 42 kg (1,225 tiles [10]) to 14.3 kg (408 tiles) making the total weight reduced by 18 kg. Note that other parts of the antenna weights about 9 kg, and the ground part (2) in Fig. 9 takes the majority. Therefore, this work achieves a successful improvement with a lighter and electrically smaller design. The proposed antenna also operates at lower frequencies than [26] and [27] and satisfies smaller electrical size *ka*. The minimum realized gain satisfies -14.5 dBi at 30.4 MHz, which is the highest among the references in the comparison table and shows an upward trend with increasing frequency. Although the electrical size is slightly larger than [23], this work represents an improved minimum realized gain in the matched band. In terms of weight, the proposed antenna is heavier compared to [26] and [27]; however, it is worth mentioning that the weight increases by about 6.3 times when the lowest matched frequency is lowered from 90 MHz [27] to 60 MHz [26], but only by 2.5 times when it is down to 30.4 MHz of this work. Overall, the proposed antenna has a much higher realized gain and relatively light weight at such a lower matched frequency, thus it can be expected to exhibit superior performance in antenna operation with the IM.

V. CONCLUSION

This study presented a low-profile, electrically small ferrite-core-loaded wideband VHF/UHF band antenna. Several constraints in the design of communication antennas for IM mounting exist, such as a low-profile form factor, vertical polarization, wideband, and lightweight. This study addressed these issues by utilizing magnetic dipole sources, ferrite cores, and optimized conductor structures. The conductor shape and placement of the ferrite cores were carefully chosen and investigated. By adding an inserted conductor, the operating frequency was shifted downward; the shape and current distribution of the antenna became similar to those of an SRR. Therefore, the overall structure of the proposed

antenna could be recognized as a single, physically large SRR unit cell and could be classified as a metamaterial-inspired antenna. The functional mechanism and radiation characteristics of the proposed antenna were also analyzed. A robust prototype was built and its performance was successfully demonstrated through experiments. According to the measurement results, the proposed antenna was matched at 30.4 MHz with a realized gain of −14.5 dBi. The ferrite tiles of the antenna weighed 14.3 kg, and the antenna satisfied the electrical size *ka* of 0.34 with an extremely thin height of 0.005λ. The proposed low-profile but electrically small antenna showed superior radiation performance compared with previously published antennas with ferrite cores [10], [23], [26], and [27]. This study presented the design, analysis, and experimental demonstration of a grounded SRR metamaterial-inspired wideband VHF/UHF communication antenna loaded with a relatively lighter weight ferrite core. The proposed antenna design is expected to be applicable in designing military communication antennas suitable for IM mounting.

REFERENCES

[1] *USS Essex*. Accessed: Sep. 1, 2023. [Online]. Available: https://www.seaforces.org/usnships/cv/CV-9-USS-Essex.htm
[2] H. Shin, D. Yoon, C. Kim, Y. S. Yang, M. G. Lee, J. Y. Park, K. C. Hwang, and Y. B. Park, "Shape optimization of an integrated mast for RCS reduction of a stealth naval vessel," *Appl. Sci.*, vol. 11, no. 6, p. 2819, Mar. 2021.
[3] B.-J. Ahn, "A study on the recent analysis method for the RCS reduction for naval ships," *J. Korean Inst. Electromagn. Eng. Sci.*, vol. 25, no. 3, pp. 333–338, Mar. 2014.
[4] X. Cheng, H. Yan, and Y. Hu, "Electromagnetic interference analysis of integrated radar antennas on stealth mast," in *Proc. 7th Asia–Pacific Conf. Environ. Electromagn. (CEEM)*, Hangzhou, China, Nov. 2015, pp. 304–308.
[5] *Saab Integrated Mast*. Accessed: Sep. 1, 2023. [Online]. Available: https://www.saab.com/products/saab-lightweight-integrated-mast
[6] R. Bijman, R. B. Timens, and F. Leferink, "Effect of integrated mast on power quality of naval vessel in island configuration," in *Proc. Int. Symp. Electromagn. Compat.*, Brugge, Belgium, Sep. 2013, pp. 489–493.
[7] L. Mattioni and G. Marrocco, "Design of a broadband HF antenna for multimode naval communications," *IEEE Antennas Wireless Propag. Lett.*, vol. 4, pp. 179–182, 2005.
[8] G. Marrocco and L. Mattioni, "Naval structural antenna systems for broadband HF communications," *IEEE Trans. Antennas Propag.*, vol. 54, no. 4, pp. 1065–1073, Apr. 2006.
[9] C. Wang, B. Yuan, J. Mao, and W. Shi, "Dual-sleeve wideband monopole antenna for shipborne systems in VHF band," *Electron. Lett.*, vol. 54, no. 19, pp. 1102–1104, Sep. 2018.
[10] W. Kim, M.-S. Lee, G. Shin, H. Kim, C.-H. Lee, Y. Kim, and I.-J. Yoon, "Ferrite-loaded, low-profile grounded bowtie-loop antenna for VHF communication," *IEEE Antennas Wireless Propag. Lett.*, early access, Sep. 5, 2023, doi: 10.1109/LAWP.2023.3311965.
[11] J. Chalas, K. Sertel, and J. L. Volakis, "Computation of the *Q* limits for arbitrary-shaped antennas using characteristic modes," *IEEE Trans. Antennas Propag.*, vol. 64, no. 7, pp. 2637–2647, Jul. 2016.
[12] T.-Y. Shih and N. Behdad, "Bandwidth enhancement of platform-mounted HF antennas using the characteristic mode theory," *IEEE Trans. Antennas Propag.*, vol. 64, no. 7, pp. 2648–2659, Jul. 2016.
[13] R. Ma, T.-Y. Shih, R. Lian, and N. Behdad, "Design of bandwidth-enhanced platform-mounted electrically small VHF antennas using the characteristic-mode theory," *IEEE Antennas Wireless Propag. Lett.*, vol. 17, no. 12, pp. 2384–2388, Dec. 2018.
[14] K. Ren, M. R. Nikkhah, and N. Behdad, "Design of dual-polarized, platform-based HF antennas using the characteristic mode theory," *IEEE Trans. Antennas Propag.*, vol. 68, no. 7, pp. 5130–5141, Jul. 2020.
[15] Y. Li, G. Yang, W. Li, and Q. H. Liu, "Dual-band antenna with OAM mode radiated by ground plane," *J. Electromagn. Eng. Sci.*, vol. 23, no. 3, pp. 244–250, May 2023.
[16] J. Won, S. Jeon, and S. Nam, "Identifying the appropriate position on the ground plane for MIMO antennas using characteristic mode analysis," *J. Electromagn. Eng. Sci.*, vol. 16, no. 2, pp. 119–125, Apr. 2016.
[17] S. R. Best and A. D. Yaghjian, "The lower bounds on q for lossy electric and magnetic dipole antennas," *IEEE Antennas Wireless Propag. Lett.*, vol. 3, pp. 314–316, 2004.
[18] A. D. Yaghjian and S. R. Best, "Impedance, bandwidth, and Q of antennas," *IEEE Trans. Antennas Propag.*, vol. 53, no. 4, pp. 1298–1324, Apr. 2005.
[19] K. Wei, Z. Zhang, and Z. Feng, "Design of a wideband horizontally polarized omnidirectional printed loop antenna," *IEEE Antennas Wireless Propag. Lett.*, vol. 11, pp. 49–52, 2012.
[20] J. Wu, S. Yang, Y. Chen, S. Qu, and Z. Nie, "A low profile dual-polarized wideband omnidirectional antenna based on AMC reflector," *IEEE Trans. Antennas Propag.*, vol. 65, no. 1, pp. 368–374, Jan. 2017.
[21] V. Rumsey and W. Weeks, "Electrically small, ferrite-loaded loop antennas," in *Proc. IRE Internat. Conv. Rec.*, New York, NY, USA, Mar. 1966, pp. 165–170.
[22] R. DeVore and P. Bohley, "The electrically small magnetically loaded multiturn loop antenna," *IEEE Trans. Antennas Propag.*, vol. AP-25, no. 4, pp. 496–505, Jul. 1977.
[23] T. Yousefi, T. Sebastian, and R. E. Diaz, "Why the magnetic loss tangent is not a relevant constraint for permeable conformal antennas," *IEEE Trans. Antennas Propag.*, vol. 64, no. 7, pp. 2784–2796, Jul. 2016.
[24] *Laird MP2106-0M0*. Accessed: Sep. 1, 2023. [Online]. Available: https://www.laird.com/products/inductive-components-emc-components-and-ferrite-cores/ferrite-plates-and-disks/mp-series/mp2106-0m0
[25] O. S. Kim, "Low-Q electrically small spherical magnetic dipole antennas," *IEEE Trans. Antennas Propag.*, vol. 58, no. 7, pp. 2210–2217, Jul. 2010.
[26] H. Moon, G.-Y. Lee, C.-C. Chen, and J. L. Volakis, "An extremely low-profile ferrite-loaded wideband VHF antenna design," *IEEE Antennas Wireless Propag. Lett.*, vol. 11, pp. 322–325, 2012.
[27] W. B. Park, S. Trinh-Van, Y. Yang, K.-Y. Lee, B. Yu, J. Park, H. You, and K. C. Hwang, "A low-profile ferrite dipole VHF antenna for integrated mast applications," *Appl. Sci.*, vol. 10, no. 5, p. 1642, Mar. 2020.

MEE-SU LEE (Student Member, IEEE) received the B.S. degree in electrical engineering from Chungnam National University, Daejeon, South Korea, in 2022, where she is currently pursuing the M.S. degree in electrical engineering. Her research interests include antennas, RF/microwave circuits, and metamaterials.

WONKYO KIM (Graduate Student Member, IEEE) received the B.S. degree in electrical engineering from Chungnam National University, Daejeon, South Korea, in 2021, where he is currently pursuing the Ph.D. degree in electrical engineering. His research interests include antennas and high-power microwave systems.

GEONYEONG SHIN received the B.S., M.S., and Ph.D. degrees in electrical engineering from Chungnam National University, Daejeon, South Korea, in 2017, 2019, and 2022, respectively. He is currently a Research Engineer with LIG Nex1, Yongin, South Korea. His research interests include antennas and theoretical methods for electromagnetics.

HYUN KIM received the B.S., M.S., and Ph.D. degrees in radio engineering from Yonsei University, Seoul, South Korea, in 2002, 2005, and 2011, respectively. He is currently a Chief Research Engineer with LIG Nex1, where he has been involved in the development of antennas for radar systems. His research interests include numerical analysis, phased array antennas, and radar systems.

CHANG-HYUN LEE received the M.S. and Ph.D. degrees in electronic information and communication engineering from Hongik University, Seoul, South Korea, in 2015 and 2020, respectively. He is currently a Research Engineer with LIG Nex1, Yongin, South Korea. His research interests include meta-structured antenna and meta-surface.

ICK-JAE YOON (Senior Member, IEEE) received the B.S. and M.S. degrees in electrical engineering from Yonsei University, Seoul, South Korea, in 2003 and 2005, respectively, and the Ph.D. degree in electrical engineering from The University of Texas, Austin, TX, USA, in 2012. He joined Chungnam National University, Daejeon, South Korea, as a Faculty Member, in 2014, where he is currently a Professor in electrical engineering. From 2012 to 2014, he was with the Electromagnetic Systems Group, Department of Electrical Engineering, Technical University of Denmark (DTU), Lyngby, Denmark, as a Postdoctoral Research Fellow and an Assistant Professor. From 2005 to 2008, he was a Research Engineer with the Samsung Advanced Institute of Technology, Samsung Electronics Company Ltd., Yongin, South Korea. His current research interests include antennas, RF/microwave circuits, electromagnetic compatibility, and theoretical methods for electromagnetics.

He received the H. C. Ørsted Postdoctoral Fellowship from DTU, in 2012. He was an Associate Editor of the *IEICE Transactions on Communications*, from 2019 to 2023.